

Modelling the Kinetics of Tartrazine Sorption by the *Rhizopus arrhizus* Biomass

Nur Adeela Yasid¹, Ain Aqilah Basirun¹, Hartinie Marbawi², Mohd Yunus Abd Shukor¹ and Mohd. khalizan Sabullah^{2*}

¹Department of Biochemistry, Faculty of Biotechnology and Biomolecular Science Universiti Putra Malaysia, 43400 UPM Serdang, Selangor, D. E, Malaysia.

²Biotechnology Programme, Faculty of Science and Natural Resources, Universiti Malaysia Sabah, 88400 Kota Kinabalu, Sabah.

*Corresponding author:

Assoc. Prof Dr. Mohd. khalizan Sabullah,
Biotechnology Programme,
Faculty of Science and Natural Resources,
Universiti Malaysia Sabah,
88400 Kota Kinabalu,
Sabah.

Email: khalizan@ums.edu.my

HISTORY

Received: 24th Sep 2022
Received in revised form: 23rd Oct 2022
Accepted: 5th Dec 2022

KEYWORDS

Adsorption
Tartrazine
Rhizopus arrhizus
Kinetics
Error function

ABSTRACT

Rhizopus arrhizus is utilized in many biotechnological applications such as in the manufacturing of enzymes, including pectinases, amylases, proteases, cellulases, and phytases, and metabolites such as lactic acid, ethanol and fumaric acids. Its spent biomass is useful in the food and feed industry. Its usage as a biosorption agent especially dye sorption is an emerging and important application. In this study we explore 16 adsorption kinetics model of tartrazine by *R. arrhizus* using nonlinear regression. Based on the statistical indicators especially penalty-based error functions such as adjusted coefficient of determination (R^2), Root-Mean-Square Error (RMSE), corrected Akaike Information Criterion (AICc), Bayesian Information Criterion (BIC), Hannan-Quinn Information Criterion (HQC) and Marquardt's percentage standard deviation (MPSD) shows that the pseudo-2nd order (PSO) was the best model followed by pseudo-nth order and Fractal-like Pseudo-2nd Order. The parameter of the PSO model gave a value of equilibrium adsorption capacity, q_e of 9.367 mg g⁻¹ (95% confidence interval (C.I.), 9.250 to 9.485) and k_2 (g/(mg.min)) of 0.037 (95%, C.I., 0.032 to 0.041). The nonlinear regression exercise allows the uncertainty determination of the parameters to be carried out.

INTRODUCTION

As a result of dye pollution, water contamination has been recognized as a severe issue worldwide [1–3]. Dye pollution sources include textile, food, paper-making, cosmetic industries, and medical and research centres [4–7]. Dye pollution is still increasing in many developing countries with less strict regulations on the manufacturing and use of dyes. Examples of these countries include Malaysia, India, Pakistan, Bangladesh, etc. [8,9]. In Malaysia, Juru riverine area was documented to have high-level contamination of dye pollution [9,10]. Effluents from dye-utilizing industries are usually released directly into the water bodies and have been a significant wastewater treatment concern [11,12]. In addition, many of the dyes and their byproducts have been documented to be mutagenic and carcinogenic, as well, as xenobiotic and recalcitrant pollutants [12–14]. Therefore, even in small amounts dyes have been reported to pose a serious threat to human health and the environment including the aquatic ecosystem [11]. Other challenges of dye pollution include increasing the chemical

oxygen demand (COD) and biological oxygen demand (BOD), compromising the photosynthesis and the aesthetic quality of the water bodies [15,16].

Dyes are highly soluble in water and because of that some of the conventional wastewater treatment processes do not effectively clean the contaminants [17,18]. Traditionally, the effective treatment of dye effluents involves combining biological, chemical, and physical processes such as; precipitation, coagulation, ion exchange, reverse osmosis, flocculation, membrane filtration, photoelectrochemistry, incineration, etc. [19]. Nevertheless, because of the excessive usage of chemicals in some cases, the implementation of these processes may significantly generate secondary metabolites or sludge [20,21]. Furthermore, these conventional methods have also been shown to have some disadvantages: high production and maintenance costs, low dye removal efficiency, and possible generation of toxic by-products [22]. Tartrazine is a dye with major uses in the food, ink and pigment industry. It is from these industries that tartrazine has been found as water pollutants

[23,24]. People who are sensitive to tartrazine, which is a yellow color that is often used in food and medicines, have been associated to having allergic responses to the drug. Individuals with allergic rhinitis, bronchial asthma, urticaria, or sensitivity to non-steroidal anti-inflammatory drugs have been shown in studies to experience significant reductions in peak expiratory flow and symptoms such as angioedema, nasal congestion, rhinorrhea, wheezing, itchy skin, and urticaria when they are given acceptable daily intake doses of tartrazine for a period of seven days [25–30]. In addition, Corder and Buckley [31] demonstrated through clinical respiratory investigations that patients who were susceptible to tartrazine suffered bronchoconstriction, which resulted in a reduction in respiratory volume. This was demonstrated by the patients' decreased lung capacity. It is anticipated that around three percent of the population, in particular those who are sensitive to salicylates, are affected by tartrazine sensitivity.

Because the chemical structure of tartrazine is comparable to that of benzoates, salicylates, and indomethacin, tartrazine may trigger allergic cross-reactions in certain individuals. Tartrazine has also been demonstrated to trigger the release of histamine in basophils of people who have chronic allergy-related diseases, such as urticaria, according to research conducted by Matsuo and colleagues [27]. In addition, Baterman and colleagues (2004) conducted an experiment with children of preschool age in which they gave them a placebo and then observed their behavior. The results of this study showed that artificial dyes, including tartrazine, have a significant influence on the hyperactive behavior of children aged three years old. These findings have also been supported by more recent research [32]. The hazardous nature of tartrazine pollution makes its removal from the environment much needed. One of the most efficient methods of dye removal at dilute levels from aquatic body is adsorption with biosorption being a cheaper alternative to expensive sorbents.

Research has been done on biosorption, and it has been hailed as a potentially useful technique for offering an environmentally friendly, cost-effective, and all-encompassing method of cleaning up a variety of environmental toxicants [33,34]. Biosorption is a physicochemical method that may be used to remove a substance (either organic or inorganic) from a solution by making use of a biological material or the components of that biological material (death or living) [35,36]. Biosorption mechanisms include adsorption, absorption, surface complexation, precipitation, and ion exchange [18,37]. It has been demonstrated that biosorption has a straightforward construction, excellent performance, user-friendliness, and a cheap overall cost.

The ingredients needed for biosorption are easy to get by (for example, waste products from agriculture and industry), and the process itself is quick, lasting anywhere from a few minutes to a few hours [38]. On various metals, dyes, and compounds in general, a great number of biosorption investigations were carried out using biomass derived from plants, animals, and other by-products [18,34]. However, many of these materials have a smaller surface area when contrasted with the surface area of bacterial biomass. As a consequence of this, the use of bacterial biomass as a solution to these issues is the primary emphasis of this investigation. One of the most cost-effective and successful strategies for removing pollutants is called bioremediation, which mostly involves biosorption. The use of microorganisms as biosorbents is intriguing for a number of reasons, including their surface area, their diversity of functional groups for sorption, their uniform size, and the fact that they may be

generated in a sustainable manner by making use of agricultural waste [39]. For example, AMT-Bioclaim™, which is made from bacterial biomass, was one of the early biosorbents for contaminants that was commercially accessible [40]. *Rhizopus arrhizus* is employed in a variety of biotechnological applications, including the production of enzymes, such as pectinases, amylases, proteases, cellulases, and phytases, as well as metabolites, such as lactic acid, ethanol, and fumaric acids, amongst other things. The food and feed sector can benefit from the discarded biomass that it produces. It is now being investigated for use as a biosorption agent, particularly for dye sorption, which is a developing and significant use. The biosorption of dyes by microorganisms, including tartrazine, is therefore a very appealing technique for reducing the effects of this pollutant. In this study we report on the kinetics of sorption of tartrazine by *Rhizopus arrhizus* inactivated biomass.

MATERIALS AND METHODS

Data Acquisition

The digitization software Webplotdigitizer, version 2.5 [41] digitized data from **Figure 3** from a published work [42]. This software gives good accuracy of extracted data and its usage has been reported in numerous publications [6, 7, 8, and 9]. The data was then nonlinearly regressed using multiple models in the curve-fitting software CurveExpert Professional, Version 2.6.5.

Kinetics models

In order to determine the adsorption kinetics constant, it is necessary to take into account both the kinetic and equilibrium areas. Because an improper choice of the initial interval time, during which the adsorption happens very quickly, can result in an inaccurate calculation of the rate constant of the PFO and PSO, it is necessary to redo the adsorption kinetics using shorter period-times, such as one minute, three minutes, five minutes, etc. Second, a common mistake is to begin with an insufficient quantity of the adsorbate or to use a diluted form of it. Because of the material's relatively low initial adsorbate concentration, not all of its adsorption sites are currently being used. Because of this difference, the value of q_e will be different from that of q_t .

Because of this, the values that were calculated for the parameters of the adsorption kinetic models, particularly the rate constants that are significant, cannot be accepted [43]. When compared to activated carbon or biochar, raw untreated biosorbent surface rarely exhibits extensive pores, which results in very low pore diffusion activities during adsorption [44–46]. Additionally, since the majority of experiments involve rapid stirring of the reaction, this reduces film diffusion to an absolute minimum. The kinetics model that was evaluated for this investigation may be found in the following (**Table 1**):

Table 1. Kinetic models for fitting the adsorption curve of tartrazine to *A. arrhizus*.

No	Kinetic model	Formula and background	Ref
1.	Pseudo-first-order	The pseudo-first model was proposed by Lagergren [47,48]. Its valid to about the first 30 min of sorption process [49]. The determination of an adequate q_e value is yet another significant challenge. Notably, the value of q_e after adjustments cannot be lower than the highest value that was observed for q_t [47,48]. The q_e value that was determined via the use of the PFO equation is not the same as the q_e value that was determined through experimentation [50]. It provides more evidence that the PFO equation is unable to adequately model the kinetic adsorption data. It	[47,48]

was hypothesized that this disparity was due to the existence of a boundary layer or an external resistance that controlled the initiation of the sorption process [49]. The linearized form has several versions that are incorrect as suggested by Tran [51]. The pseudo-first-order kinetic model equation is as follows [52]:

$$q_t = q_e(1 - e^{-k_1 t})$$

It is the first model that describes the kinetic rate of the liquid-solid phase for the adsorption process based on the adsorption capacity, and it has the distinction of being the first model to do so. It is the kinetic model that has been used the second most frequently to illustrate that the driving force is proportional to the available percentage of active sites. This model provides further evidence that the chemisorption process is at play.

2. Pseudo-second-order [54] The pseudo-second-order model is one that is based on the adsorption capacity onto a solid phase, and Blanchard et al. were the ones who first presented the nonlinear form of the PSO model [53]. It is expressed as:

$$q_t = \frac{k_2 q_e^2 t}{1 + k_2 q_e t}$$

Where k_2 (g/(mg.min)) is the pseudo-second-order rate constant

The rate of change in adsorption capacity slows down in a manner that is exponentially relative to the quantity of adsorbate that has been adsorbed.

3. Elovich [55] Simulation of the adsorption of carbon monoxide on the sorbent manganese dioxide was the original driving force behind the development of the Elovich equation. The Elovich model is expressed as follow.

$$q_t = \frac{1}{\beta \ln a \beta} + \frac{1}{\beta \ln t}$$

Where, a is the initial sorption rate (mg/g.min⁻¹) and β is surface coverage extent (g.mg⁻¹) and chemisorption activation energy. Datapoint that starts from the origin (0,0) must be removed due to the \ln term.

4. Mixed 1,2-order [56,57] A type of pseudo-first-order and pseudo-second-order kinetic equations that is mixed together. This model, which is a linear combination of the pseudo-first-order and the pseudo-second-order equations, is referred to as the mixed 1,2-order equation (MOE). The formula is as follow.

$$q_t = q_e \left\{ 1 - \frac{k_1 \exp(-k_1 t)}{k_1 + q_e k_2 (1 - \exp(-k_1 t))} \right\}$$

Where k_1 and k_2 , represent first- and second-order kinetics, respectively.

5. Fractal-like pseudo-first order [58] Incorporating the fractal concept into the pseudo-first-order model was one of the suggested modifications to the model. The formula is as follow.

$$q_t = q_e [1 - \exp(-k_1' t^\phi)]$$

Here the adsorption rate coefficient might have a temporal dependency during the adsorption time. ϕ is the fractal time exponent and k_1' (1/min ^{ϕ}) is the fractal-like pseudo-first-order rate constant.

6. Fractal-like pseudo-second order [58] In a similar vein, an additional modification for the pseudo-second-order model has been suggested, and this time it involves the concept of fractals. The formula is as follow.

$$q_t = \frac{k_2' q_e^2 t^\phi}{1 + k_2' q_e t^\phi}$$

k_1' (g/(mg min) ^{ϕ}) and ϕ are the fractal-like pseudo-second-order rate constant and exponent, respectively.

7. Pseudo-nth order [59] It can be difficult to discern the order of the adsorption process in particular circumstances.

This indicates that the PSO and PFO models are able to adequately fit the experience data of time dependency. Because of this, the pseudo-nth-order (PNO) model or the general order kinetic (GOK) model is also utilized in order to accurately identify the overall order of the adsorption process.

$$q_t = q_e - \frac{q_e}{[k_N (q_e)^{n-1} t(n-1) + 1]^{\frac{1}{1-n}}}; n \neq 1$$

Where, n is the order of kinetic adsorption (n could be an integer or non-integer rational number) and k_N is the general order rate constant ((g/mg) ^{$n-1$} /min),

8. One-site Langmuir [60] The kinetic model works on the assumption that the overall adsorption rate is simply the difference between the adsorption and desorption rates, and that once equilibrium is reached, these two rates cancel each other out to give the same result.

While the rate of desorption is related to the amount that was adsorbed, the rate of adsorption is proportional to the solute concentration that is already present in the bulk phase and the amount of accessible adsorbent surface. The formula is as follow.

$$q_t = q_e \left[\frac{K'_{ad}}{(K'_{ad} + K_d)} \right] \left\{ 1 - \exp[-(K'_{ad} + K_d)t] \right\}$$

K'_{ad} is the Langmuir adsorption rate constant (1/min) and K_d is the desorption rate constant (1/min)

9. Modified-Freundlich [61] The Freundlich equation was modified to include a time-dependent expression, which allowed for the development of a kinetic model. The formula is as follow.

$$q_t = k C_0 t^{\frac{1}{n}}$$

where k is the apparent adsorption rate constant (L/g.min ^{$1/n$}); n is the Kuo-Lotse constant; C_0 is the initial adsorbate concentration (mmol/L); and t is the adsorption time

10. Avrami [62] Under the premise that nucleation occurs in a manner that is spatially random, this model predicts the kinetics of phase transition. This provides an illustration of the kinetic parameters as feasible variations of the adsorption rates in terms of the initial concentration and the adsorption period. Additionally, it provides an evaluation of fractional kinetic orders. The formula is as follow.

$$q_t = q_e \{ 1 - \exp[-(k_{Av} t)^{n_{Av}}] \}$$

the Avrami kinetic model rate constant (1/min) and n_{Av} (fraction) is the model exponent of time related to the adsorption mechanism changes.

11. Exponential [63] An exponential form of the kinetic equation is a form of the equation that can be used to illustrate the pattern of an adsorption rate as a function of time. Between pseudo-first-order models and pseudo-second-order models is where the driving force of the exponential model rests. Both homogeneous and heterogeneous surfaces are appropriate contexts for using the kinetic model. The formula is as follow.

$$\frac{q_t}{q_e} = \ln [2.72 - 1.72 \exp(-k_{Exp} t)]$$

k_{Exp} is the exponential kinetic model rate constant (mg/(g.min)). Datapoint that starts from the origin (0,0) must be removed due to the \ln term.

12. Double-exponential Wilczak and Keinath came up with a double exponential kinetic model after observing the kinetics of copper(II) and lead(II) adsorption on activated carbon. This model was based on their results. This equation describes the adsorption characteristics as a two-step mechanism, with the first step being a quick phase that includes both internal and exterior diffusions. This is preceded by a slow phase that is governed by the intra-particle diffusion. The formula is as follow. [64]

$$q_t = q_e - \frac{D_R}{m_{ads}} \exp(-k_{DR}t) - \frac{D_S}{m_{ads}} \exp(-k_{DS}t)$$

Where, K_{DR} and K_{DS} are diffusion parameters (1/min) for the rapid and slow step of double-exponential model, respectively, m_{ads} is the adsorbent amount in the solution (g/L) and D_R and D_S are adsorption rate parameters of the rapid and the slow step (mmol/L), respectively.

13. Hyperbolic tangent The hyperbolic tangent function has been used as the foundation for the development of this mathematical model. In addition to this, it is able to calculate the precise equilibrium time of the adsorption process. The formula is as follow. [65]

$$\frac{q_t}{q_e} = \left[\tanh \left(\pi \frac{t}{t_{eHT}} \right) \right]^{n_{HT}}$$

t_{eHT} is the required time for adsorption to reach the equilibrium state (min) and n_{HT} represents the adsorbent surface heterogeneity.

14. Brouers and Sotolongo a time dependent rate or hazard function (in reliability theory) or intensity of transition (in relaxation theory), $R(t)$. The formula is as follow. [67]

$$y = qe \left[1 - \left(1 + (n-1) \left(\frac{t}{\tau} \right)^\alpha \right)^{-\frac{1}{n-1}} \right]$$

Musawi suggests to use (n, a) of (1.5, a). The formula is as follow.

$$y = qe \left[1 - \left(1 + (0.5) \left(\frac{t}{\tau} \right)^\alpha \right)^{-2} \right]$$

Where n is the reaction's fractional order; α is the fractal coefficient that, on a macro scale, expresses the level of complexity of the sorbent-sorbate relationship, and τ is the characteristic time (min). It has been suggested for the whole series to use $B_{\mathcal{Y}}$ (1.5.a) [66].

15. normalized Gudermannian function In order to simulate the sigmoidal shape of sorption kinetics data, the normalized Gudermannian function was introduced. The function is related to both the circular and the hyperbolic functions. The formula is as follow. [68]

$$\frac{q_t}{q_e} = \left\{ 0.637 \tan^{-1} \left[\sinh \frac{5.233 \times t}{t_{eG}} \right] \right\}^{n_G}$$

where t_{eG} reflects the amount of time that must have passed for the adsorption process to reach the condition of equilibrium and the heterogeneity of the adsorption system is represented by the parameter n_G .

16. Sigmoidal Chapman In addition to that, the Sigmoidal Chapman model was incorporated into this study. It is depicted by the equation: where the adsorption rate constant is denoted by b (h^{-1}), and c represents how the adsorption rate varies as a function of time. The formula is as follow. [69]

$$q_t = q_e(1 - e^{-bt})^c$$

The idea that adsorbate molecules interact with one another in a cooperative manner forms the foundation of the equivalent Chapman isotherm model.

Note
 q_e is the time dependent and maximum sorbed quantities (mg/g)
 t is time (min)

Statistical analysis

To determine if there is a significant difference in terms of fitness among models with varying numbers of parameters, statistics functions such as the adjusted coefficient of determination (R^2), Root-Mean-Square Error (RMSE), corrected Akaike Information Criterion (AICc), Bayesian Information Criterion (BIC), Hannan-Quinn Information Criterion (HQC), bias factor, and accuracy factor (BF, AF) were applied to the same set of experimental data. The RMSE, which accounts for the penalty for the number of parameters, was calculated using Eqn 1, where n is the number of experimental data, p is the number of parameters, Ob_i is the experimental data, and Pd_i is the value predicted by the model [70].

$$RMSE = \sqrt{\frac{\sum_{i=1}^n (Pd_i - Ob_i)^2}{n-p}} \quad (\text{Eqn. 1})$$

To determine the validity of the models, both BF and AF were used. The Bias Factor should be set to 1 to achieve a correlation of 1 between the predicted and observed values. If the Bias Factor (as shown in Equation 2) is greater than 1, it indicates a fail-safe model, and if it is less than 1, it indicates a fail-negative model. If Accuracy is less than 1, it means that the prediction will be less accurate (Eqn. 3).

$$Bias\ factor = 10 \left(\sum_{i=1}^n \log \frac{(Pd_i/Ob_i)}{n} \right) \quad (\text{Eqn. 2})$$

$$Accuracy\ factor = 10 \left(\sum_{i=1}^n \log \frac{|(Pd_i/Ob_i)|}{n} \right) \quad (\text{Eqn. 3})$$

In linear regression, the best fitting model was determined by R^2 or coefficient of determination. However, in nonlinear regression, the R^2 does not give a comparative analysis where the number of parameters between models is different. To overcome this, adjusted R^2 was used to calculate the quality of the nonlinear models. In the adjusted R^2 formula, S_y^2 is the total variance of the y-variable and RMS is Residual Mean Square (Eqns. 4 and 5).

$$Adjusted\ (R^2) = 1 - \frac{RMS}{S_y^2} \quad (\text{Eqn. 4})$$

$$Adjusted\ (R^2) = 1 - \frac{(1-R^2)(n-1)}{(n-p-1)} \quad (\text{Eqn. 5})$$

Various statistical models can be evaluated for a given range of experimental data using the Akaike Information Criterion (AIC). Alternatively, AICc (the corrected AIC) should be used for data sets with numerous parameters or a few data point values [71]. The AICc was calculated based on the following Eqn. 6.

$$AICc = 2p + n1n \left(\frac{RSS}{n} \right) + 2(p+1) + \frac{2(p+1)(p+2)}{n-p-2} \quad (\text{Eqn. 6})$$

The AICc gives information about the differences that exist between the two models in terms of the number of parameters (p) and the fitting. The AICc value that is the smallest possible would suggest the model that best fits the data [71]. A further information-theory-based approach to statistics is the Bayesian Information Criterion (Eqn. 7). The number of parameters is punished more harshly by this error function than it is by AIC [72].

$$BIC = n \cdot \ln \frac{RSS}{n} + p \cdot \ln(n) \quad (\text{Eqn. 7})$$

The Hannan–Quinn information criterion, often known as the HQC, is an additional error function approach that relies on the information theory (Eqn. 8). In contrast to the AIC, the HQC exhibits a high level of consistency because the equation contains the $\ln \ln n$ term. [73];

$$HQC = n \times \ln \frac{RSS}{n} + 2 \times p \times \ln(\ln n) \quad (\text{Eqn. 8})$$

Another is MPSD. The Marquardt’s percent standard deviation (MPSD). This error function distribution follows the geometric mean error which allows for the penalty to the number of parameters of a model (Eqn. 9).

$$MPSD = 100 \sqrt{\frac{1}{n-p} \sum_{i=1}^n \left(\frac{Ob_i - Pd_i}{Ob_i} \right)^2} \quad (\text{Eqn. 9})$$

where n is the number of experimental data, p is the number of parameters, Ob_i is the experimental data, and Pd_i is the value predicted by the model

RESULTS AND DISCUSSION

Determination of kinetic model for batch adsorption studies

Since the linearisation of nonlinear data disturbs the data's error structure, this makes it harder to assess uncertainty, which is often reported as 95% confidence interval range [74]. Hence, the non-linear regression is preferable for kinetic model fitting since it is conducted on the same abscissa with a linear regression plot, showing more accurate calculations. The various kinetic models utilized in this study (Figs. 1 to 16) shows visually acceptable fittings for all tested models.

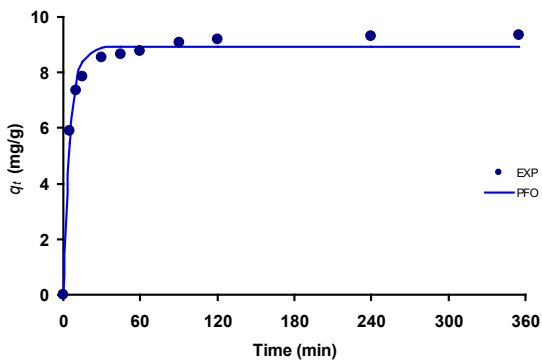


Fig. 1. Experimental data versus calculated data (line) of tartrazine dye adsorption using *Rhizopus arrhizus* as modelled using the pseudo-first order model.

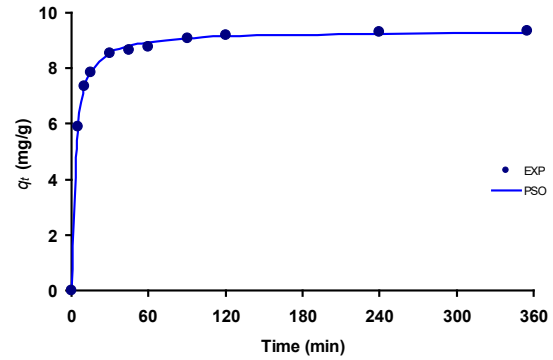


Fig. 2. Experimental data versus calculated data (line) of tartrazine dye adsorption using *Rhizopus arrhizus* as modelled using the pseudo-second order model.

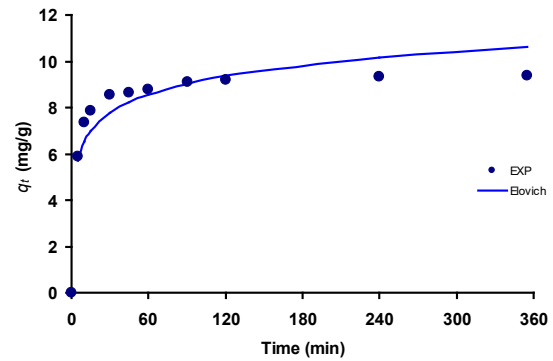


Fig. 3. Experimental data versus calculated data (line) of tartrazine dye adsorption using *Rhizopus arrhizus* as modelled using the Elovich model.

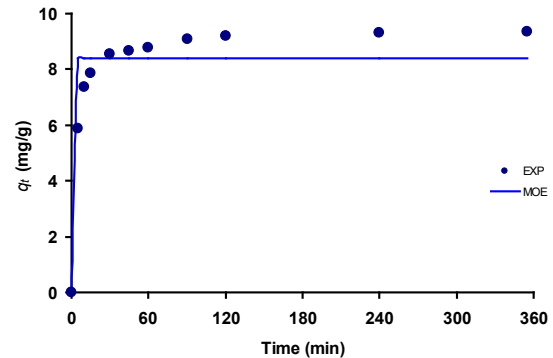


Fig. 4. Experimental data versus calculated data (line) of tartrazine dye adsorption using *Rhizopus arrhizus* as modelled using the mixed order (MOE) model.

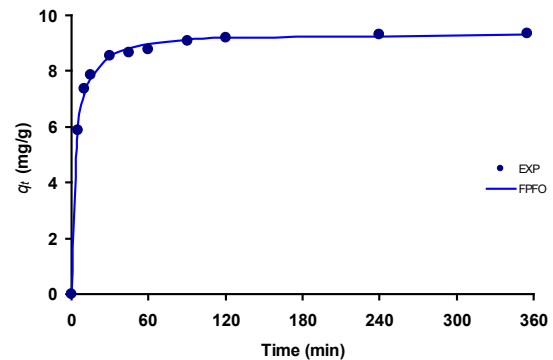


Fig. 5. Experimental data versus calculated data (line) of tartrazine dye adsorption using *Rhizopus arrhizus* as modelled using the fractal pseudo-first order model.

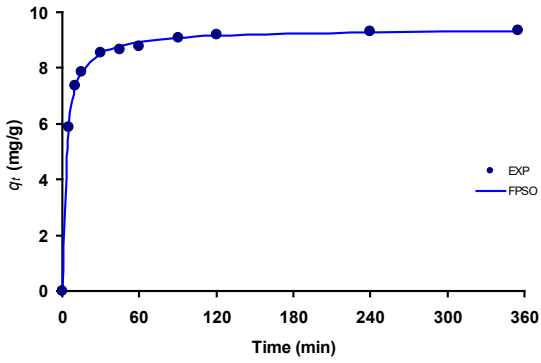


Fig. 6. Experimental data versus calculated data (line) of tartrazine dye adsorption using *Rhizopus arrhizus* as modelled using the fractal pseudo-second order model.

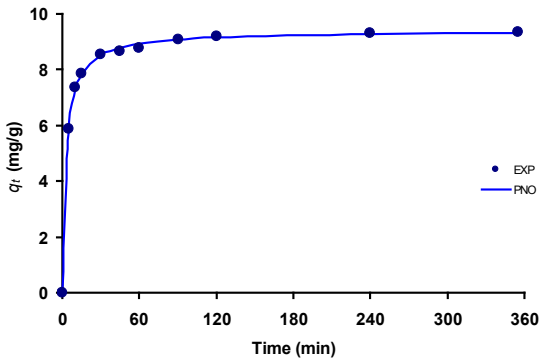


Fig. 7. Experimental data versus calculated data (line) of tartrazine dye adsorption using *Rhizopus arrhizus* as modelled using the fractal pseudo-nth order model.

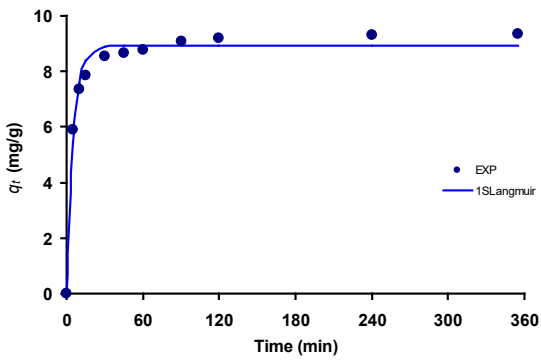


Fig. 8. Experimental data versus calculated data (line) of tartrazine dye adsorption using *Rhizopus arrhizus* as modelled using the one-site Langmuir model.

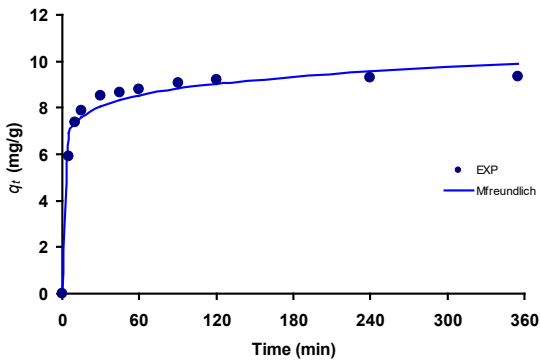


Fig. 9. Experimental data versus calculated data (line) of tartrazine dye adsorption using *Rhizopus arrhizus* as modelled using the modified Freundlich model.

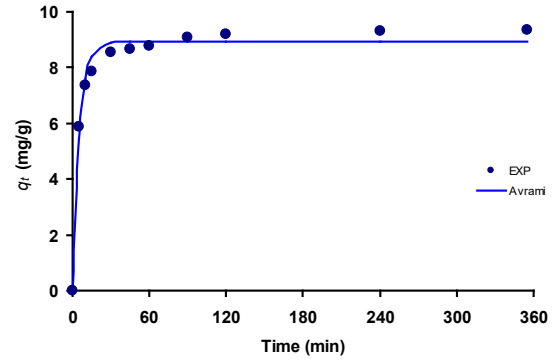


Fig. 10. Experimental data versus calculated data (line) of tartrazine dye adsorption using *Rhizopus arrhizus* as modelled using the Avrami model.

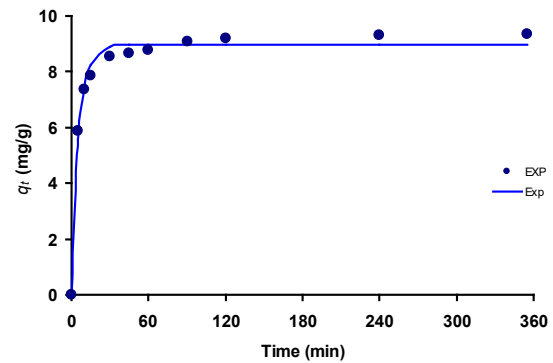


Fig. 11. Experimental data versus calculated data (line) of tartrazine dye adsorption using *Rhizopus arrhizus* as modelled using the exponential model.

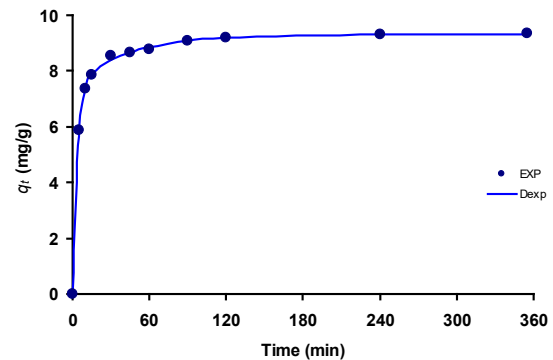


Fig. 12. Experimental data versus calculated data (line) of tartrazine dye adsorption using *Rhizopus arrhizus* as modelled using the double-exponential model.

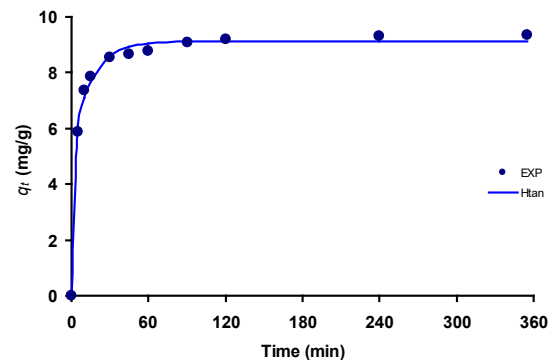


Fig. 13. Experimental data versus calculated data (line) of tartrazine dye adsorption using *Rhizopus arrhizus* as modelled using the hyperbolic tangent model.

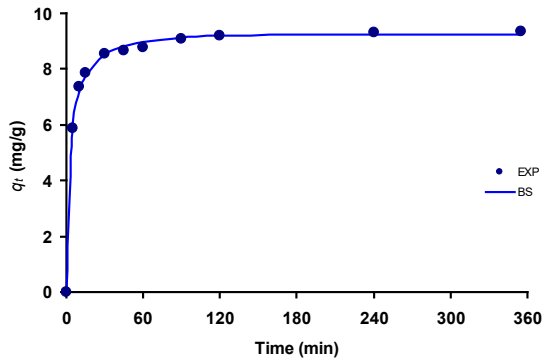


Fig. 14. Experimental data versus calculated data (line) of tartrazine dye adsorption using *Rhizopus arrhizus* as modelled using the Brouers and Sotolongo model.

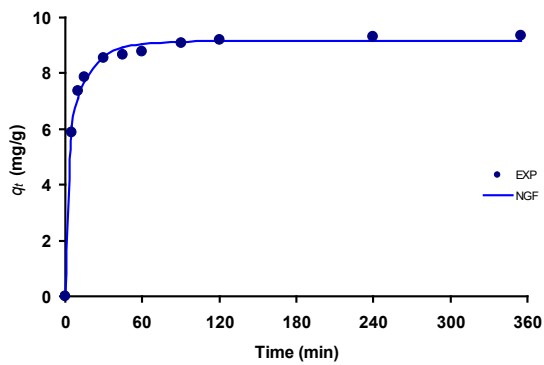


Fig. 15. Experimental data versus calculated data (line) of tartrazine dye adsorption using *Rhizopus arrhizus* as modelled using the normalized Gudermannian function model.

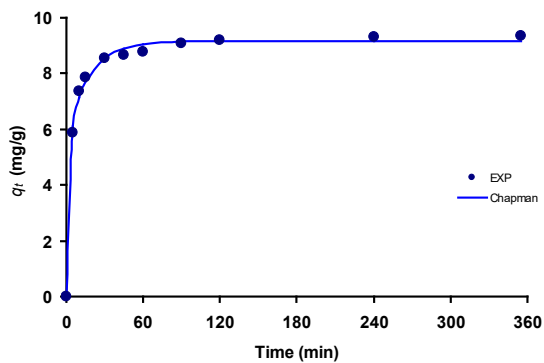


Fig. 16. Experimental data versus calculated data (line) of tartrazine dye adsorption using *Rhizopus arrhizus* as modelled using the sigmoidal Chapman model.

Based on the statistical indicators especially penalty-based error functions such as AICc, AdjR², BIC, HQC and MPSD shows that the pseudo-2nd order was the best model followed by pseudo-nth order and Fractal-like Pseudo-2nd Order (**Table 2**). Kinetic analysis using the PSO model gave a value of equilibrium adsorption capacity, q_e of 9.367 mg g⁻¹ (95% confidence interval (C.I.), 9.250 to 9.485) and k_2 (g/(mg.min)) of 0.037 (95%, C.I., 0.032 to 0.041) (**Table 2**). The result of the nonlinear regression work was within the range of the original study at 9.28 mg g⁻¹ and 0.026.

As far as tartrazine biosorption is concerned (**Table 4**), the PSO model is also the best model for several adsorbents such as *Inula viscosa* waste [75], activated carbon derived from *Cassava sievate* biomass [76], iron nanoadsorbents utilizing different waste plant biomass [77], lanthanum enriched aminosilane-grafted mesoporous carbon material [78], magnetic Ni-Ag bimetallic nanoparticles supported on reduced graphene oxide (Ni-Ag NPs/rGO) [79], activated carbon produced from pecan nut shells [80], masau stone (MS) [81], copper coordinated dithiooxamide metal-organic framework (Cu-DTO MOF) [82], Fe(II) based adsorbent system [83], iron modified zeolitic tuff [84], activated carbon from Alligator weed (*Alternanthera philoxeroides*) [85], polyaniline nanolayer composite [86], while the PFO was the best model for adsorption of tartrazine using natural quartz, modified with a cationic surfactant and homoionized with sodium [87] ZnAl-LDH/PVA nanocomposite [88].

Table 2. Statistical analysis for tartrazine adsorption using *Rhizopus arrhizus* adsorbent at 100 mg/L dye.

Model	p	RMSE	adR2	MPSD	AICc	BIC	HQC	BF	AF
Pseudo-first-order	2	0.363	0.980	105.41	-11.07	-19.71	-21.00	0.998	1.023
Pseudo-second-order	2	0.088	0.999	1.04	-42.25	-50.88	-52.18	1.000	1.008
Elovich	2	0.827	0.886	8.70	7.04	-1.60	-2.89	0.980	1.036
Mixed 1	3	1.158	0.761	13.78	20.39	6.92	4.97	1.008	1.056
Fractal-like pseudo-1st order	3	0.149	0.997	1.97	-24.73	-38.20	-40.15	1.000	1.010
Fractal-like pseudo-second order	3	0.091	0.999	1.13	-35.63	-49.10	-51.05	1.000	1.007
Pseudo-nth order	3	0.088	0.999	1.12	-36.39	-49.86	-51.81	1.000	1.007
One-site Langmuir	3	0.385	0.98	4.94	-3.84	-17.31	-19.26	0.998	1.023
Modified-Freundlich	2	0.471	0.966	6.19	-5.34	-13.97	-15.27	1.003	1.027
Avrami	3	0.385	0.978	4.94	-3.84	-17.31	-19.26	0.998	1.023
Exponential	2	0.304	0.986	3.76	-14.97	-23.60	-24.90	0.998	1.022
Double-exponential	5	0.074	0.999	0.90	-20.98	-51.99	-55.23	1.000	1.002
Hyperbolic tangent	3	0.225	0.992	2.86	-15.63	-29.10	-31.05	1.001	1.017
Brouers and Sotolongo normalized Gudermannian function	3	0.149	0.997	1.97	-24.73	-38.20	-40.15	1.000	1.010
Sigmoidal Chapman	3	0.199	0.994	2.56	-18.37	-31.85	-33.79	1.001	1.014

Table 3. Model constants for the top-three kinetic models for tartrazine adsorption using *Rhizopus arrhizus* adsorbent at 100 mg/L dye.

Model	value	(95% C.I.)
Pseudo-2 nd order		
q_e (mg/g)	9.367	9.250 to 9.485
k_2 (g/(mg.min))	0.037	0.032 to 0.041
Pseudo-nth order		
q_e (mg/g)	9.393	9.136 to 9.651
k_N ((g/mg)n ⁻¹ /min)	-3.632	-7.577 to 0.313
n	-0.043	-0.419 to 0.33
Fractal-like Pseudo-2 nd Order		
q_e (mg/g)	9.323	9.151 to 9.495
k'_2 (g/(mg min)) ^φ	0.034	0.024 to 0.043
$φ$	1.051	0.892 to 1.210

It was often accepted that the ability to fit the kinetic data was the best test of the PFO and PSO equations' validity, despite the fact that such a test has little to do with whether or not the equations have a solid physicochemical foundation. Both k_1 and k_2 were phenomenological rate constants that declined when the adsorbate concentration was raised at the outset. k_1 and k_2 values varied widely from measurement to measurement, making it difficult to draw conclusions about the underlying physics and chemistry and extrapolate valuable results.

The PFO and PSO equations may be fitted to most kinetic data even if the experimental conditions affecting the adsorption kinetics were not completely controlled. The PFO equation typically gave lower estimates of q_e than did the experiments. This mismatch was due to a delay in the onset of the adsorption process, which was likely brought on by the existence of a

boundary layer or external resistance regulating. In the adsorption process that followed the PSO equation, the chemical reaction is not always the rate-limiting step because a good fit alone is not enough to reveal the true nature of the rate-limiting step [57,89,90].

Table 4. Summary of tartrazine dye sorption by sorbents.

Adsorbent	Best kinetics	Ref.
<i>Imula viscosa</i> waste	PSO	[75]
activated carbon derived from <i>Cassava sievate</i> biomass	PSO	[76]
iron nanoadsorbents utilizing different waste plant biomass	PSO	[77]
lanthanum enriched aminosilane-grafted mesoporous carbon material	PSO	[78]
magnetic Ni-Ag bimetallic nanoparticles supported on reduced graphene oxide (Ni-Ag NPs/rGO)	PSO	[79]
activated carbon produced from pecan nut shells	PSO	[80]
mascopper coordinated dithiooxamide metal-organic framework (Cu-DTO MOF)	PSO	[82]
Fe(II) based adsorbent system	PSO	[83]
iron modified zeolitic tuff	PSO	[84]
activated carbon from Alligator weed (<i>Alternanthera philoxeroides</i>)	PSO	[85]
polyaniline nanolayer composite	PSO	[86]
masau stone (MS)	PSO	[81]
Activated carbon of <i>Lantana camara</i>	PSO	[99]
Crosslinked Chitosan-Coated Bentonite	PSO	[100]
natural quartz, modified with a cationic surfactant and homoionized with sodium	PFO	[87]
ZnAl-LDH/PVA nanocomposite	PFO	[88]
hen feathers	PFO	[101]
Deoiled soya waste	PFO (default)	[102]
Bottom ash from thermal power	PFO (default)	[102]
Chitin and Chitosan	Avrami	[103]

Note:
 PSO Pseudo-2nd order
 PFO Pseudo-1st order

Analytical methods, as well as data on adsorptive thermodynamics such as changes in entropy and enthalpy, activation- and adsorption energies, are required in order to determine whether the adsorption of pollutants in solution is a physical or chemical process [51]. Both of the kinetic models for sorption from liquid solutions were obtained without any process conditions being treated as particularly important. The creation of these models from theory is presented in detail by Azizian, who also provides the support of experimental findings in his analysis.

The model's theoretical derivation has the benefit of providing an estimation of the circumstances necessary to offer a more expressive interpretation of kinetic parameters. This is possible because of the models' ability to predict the conditions that must be satisfied. Azizian has noticed that the PFO kinetic model's observed rate constant (k_1) symbolizes a mix of desorption and adsorption rate constants, and not the rate constant's intrinsic adsorption [91]. This is because k_1 does not the rate constant's intrinsic adsorption. In the study of sorption kinetics, the PFO model can account for the use of high starting solute concentration (C_0) of the adsorbate, but the PSO model can more consistently suit low values of C_0 .

The PFO model can also account for the use of low values of C_0 . For adsorption profiles that obey the PFO kinetic model, the observed k_1 value is linearly proportionate to the initial solute concentration, where the intercept and slope imply the desorption and adsorption rate constants, respectively. This is the case for adsorption profiles that follow the PFO kinetic model. The observed rate constant is a convoluted function of the initial

sorbate concentration in the scenario in which processes of adsorption follow PSO kinetics [91].

To reiterate, the PFO model is supported by experimental studies whenever the solute's initial concentration is high. In contrast, when the solute concentration is low, the PSO kinetic model is dominant [91–96]. Additionally, the intraparticle diffusion model is one of several kinetic models of adsorption that have been used to investigate the adsorption process at the atomic and molecular levels, especially for porous sorbents [97,98]. If chemical sorption or chemisorption is assumed to be the rate-limiting phase, then the PSO kinetic model may predict behavior across the whole adsorption range. As a result of this circumstance, the adsorption rate is independent of the adsorbate concentration and instead is dependent on the adsorption capacity.

The equilibrium adsorption capacity can be calculated with this model, which is a huge improvement over the Lagergren first order model. Therefore, in principle, there is no need to use experimental data to evaluate the adsorption equilibrium capacity. As the concentration of the solute at the outset grows, the correlation between the data and the PSO kinetics model decreases, while the data and the PFO model grow increasingly well-fitted [91].

CONCLUSION

Linearized form of adsorption kinetics has its drawbacks such as inaccurate representation of 95% confidence interval output of the parameters, transformation activity give unbalanced attention to potential outliers and magnification of errors may result in inaccurate parameters value. In this study we explore 16 adsorption kinetics model of tartrazine by *R. arrhizus* using nonlinear regression. Based on the statistical indicators especially penalty-based error functions such as AICc, ADR2, BIC, HQC and MPSD shows that the pseudo-2nd order (PSO) was the best model followed by pseudo-nth order and Fractal-like Pseudo-2nd Order. Kinetic analysis using the PSO model gave a value of equilibrium adsorption capacity, q_e of 9.367 mg g⁻¹ (95% confidence interval (C.I.), 9.250 to 9.485) and k_2 (g/(mg.min)) of 0.037 (95%, C.I., 0.032 to 0.041).

REFERENCES

- Jayanth N, Karthik R, Logesh S, K SR, Vijayanand K. Environmental issues and its impacts associated with the textile processing units in. 2nd Int Conf Environ Sci Dev IPCBEE. 2011;4(17):120–4.
- Kurade MB, Awasthi MK, Govindwar SP, Jeon BH, Kalyani D. Editorial: Microbiotechnology Tools for Wastewater Cleanup and Organic Solids Reduction. Front Microbiol. 2021;12(February):10–2.
- Singh KP, Gupta S, Singh AK, Sinha S. Optimizing adsorption of crystal violet dye from water by magnetic nanocomposite using response surface modeling approach. J Hazard Mater. 2011;186(2–3):1462–73.
- Chavan RB. Indian textile industry - Environmental issues. Indian J Fibre Text Res. 2001;26(1–2):11–21.
- Kalme SD, Parshetti GK, Jadhav SU, Govindwar SP. Biodegradation of benzidine based dye Direct Blue-6 by *Pseudomonas desmolyticum* NCIM 2112. Bioresour Technol. 2007;98(7):1405–10.
- Kumar P, Bhati H, Rani A, Singh R. Role of Biosorption of Dyes and Microorganisms in Environment. Life Sci. 2015;4(2):38–41.
- Mohan S, Muralimohan N, Vidhya K, Sivakumar CT. a Case Study on-Textile Industrial Process, Characterization and Impacts of Textile Effluent. Indian JSciRes. 2017;17(1):80–084.
- Islam MM, Mahmud K, Faruk O, Billah S. Assessment of environmental impacts for textile dyeing industries in Bangladesh.

- Proc Int Conf Green Technol Environ Conserv GTEC-2011. 2011;2(6):173–81.
9. Izuan M, Halmi E, Gunasekaran B, Razi Othman A, Dahalan FA. A rapid inhibitive enzyme assay for monitoring heavy metals pollution in the Juru Industrial Estate [Internet]. Vol. 3, Bioremediation Science and Technology Research. 2015 [cited 2021 Jun 11]. p. 7–12. Available from: <http://journal.hibiscuspublisher.com/index.php/BSTR/index>
 10. Manogaran M, Yasid NA, Othman AR, Gunasekaran B, Izuan M, Halmi E, et al. Biodecolourisation of Reactive Red 120 as a Sole Carbon Source by a Bacterial Consortium-Toxicity Assessment and Statistical Optimisation. *Public Health*. 2021;18:2424.
 11. Lellis B, Fávoro-polonio CZ, Pamphile JA, Polonio JC. Effects of textile dyes on health and the environment and bioremediation potential of living organisms. 2019;
 12. Puvaneswari N, Muthukrishnan J, Gunasekaran P. Toxicity assessment and microbial degradation of azo dyes. *Indian J Exp Biol*. 2006;44(8):618–26.
 13. Karim ME, Dhar K, Hossain MT. Decolorization of Textile Reactive Dyes by Bacterial Monoculture and Consortium Screened from Textile Dyeing Effluent. *J Genet Eng Biotechnol*. 2018;16(2):375–80.
 14. Şenol ZM. Effective biosorption of Allura red dye from aqueous solutions by the dried-lichen (*Pseudoevernia furfuracea*) biomass. *Int J Environ Anal Chem*. 2020;00(00):1–15.
 15. El-Idreesy TT, Khoshala O, Firouzi A, Elazab HA. Equilibrium and kinetic study on the biosorption of trypan blue from aqueous solutions using avocado seed powder. *Biointerface Res Appl Chem*. 2021;11(3):11042–53.
 16. Walker GM, Weatherley LR. Biodegradation and biosorption of acid anthraquinone dye. *Environ Pollut*. 2000;219–23.
 17. Vijayaraghavan K, Yun Y sang. Utilization of fermentation waste (*Corynebacterium glutamicum*) for biosorption of Reactive Black 5 from aqueous solution. 2007;141:45–52.
 18. Vijayaraghavan K, Yun YS. Bacterial biosorbents and biosorption. *Biotechnol Adv*. 2008;26(3):266–91.
 19. Wang Y, Jiang L, Shang H, Li Q, Zhou W. Environmental Technology & Innovation Treatment of azo dye wastewater by the self-flocculating marine bacterium *Aliiglaciecola lipolytica*. *Environ Technol Innov*. 2020;19:100810.
 20. Chang JS, Chou C, Lin YC, Lin PJ, Ho JY, Lee Hu T. Kinetic characteristics of bacterial azo-dye decolorization by *Pseudomonas luteola*. *Water Res*. 2001;35(12):2841–50.
 21. Lade H, Kadam A, Paul D, Govindwar S. A Low-Cost Wheat Bran Medium for Biodegradation of the Benzidine-Based Carcinogenic Dye Trypan Blue Using a Microbial Consortium. 2015;3480–505.
 22. Ismail M, Akhtar K, Khan MI, Kamal T, Khan MA, M. Asiri A, et al. Pollution, Toxicity and Carcinogenicity of Organic Dyes and their Catalytic Bio-Remediation. *Curr Pharm Des*. 2019;25(34):3645–63.
 23. Shiralipour R, Larki A. Pre-concentration and determination of tartrazine dye from aqueous solutions using modified cellulose nanospheres. *Ecotoxicol Environ Saf*. 2017 Jan 1;135:123–9.
 24. Methneni N, González JAM, Van Loco J, Anthonissen R, de Maele JV, Verschaeve L, et al. Ecotoxicity profile of heavily contaminated surface water of two rivers in Tunisia. *Environ Toxicol Pharmacol*. 2021 Feb 1;82:103550.
 25. Bateman B, Warner JO, Hutchinson E, Dean T, Rowlandson P, Gant C, et al. The effects of a double blind, placebo controlled, artificial food colourings and benzoate preservative challenge on hyperactivity in a general population sample of preschool children. *Arch Dis Child*. 2004 Jun 1;89(6):506–11.
 26. Doguc D, Aktas A, Gazioglu N, Kocabas CN. Tartrazine and other azo dyes: a review of literature. *Food Chem Toxicol*. 2013;62:340–50.
 27. Matsuo H, Kato K, Ohno Y, Kato S. The effect of tartrazine on histamine release from human basophils. *Allergol Int*. 2013;62(4):539–47.
 28. Khayyat MA, Al-Qahtani JA, Al-Saleh YA, Al-Mofleh IA. The prevalence of food additives intolerance in adult patients with chronic urticaria. *Int J Dermatol*. 2017;56(5):536–41.
 29. Bhatt S, Kamat D. The Role of Tartrazine in the Development of Asthma and Allergic Rhinitis in Children. *J Allergy Clin Immunol Pract*. 2018;6(4):1251–8.
 30. Ara L, Caldas J, Flávia M, Marmo VC, Patrícia Costa CD, et al. Hormesis in tartrazine allergic responses of atopic patients: An overview of clinical trials and a raw data revision. *Environ Dis*. 2020 Jul 1;5(3):59–59.
 31. Corder R, Buckley D. Tartrazine and respiratory symptoms. *Thorax*. 1995;50(6):663–6.
 32. Yong SB, Gau SY, Guo YC, Wei JCC. Allergy from perspective of environmental pollution effects: from an aspect of atopic dermatitis, immune system, and atmospheric hazards—a narrative review of current evidences. *Environ Sci Pollut Res*. 2022 Aug 1;29(38):57091–101.
 33. Abdi O, Kazemi M. A review study of biosorption of heavy metals and comparison between different biosorbents. *J Mater Environ Sci*. 2015;6(5):1386–99.
 34. Crini G, Lichtfouse E. Green adsorbents for pollutant removal: fundamentals and design [Internet]. 2018. 390 p. Available from: https://books.google.pt/books?id=BVhDwAAQBAJ&dq=model+Spahn+%26+Schlunder+sorption&hl=pt-PT&source=gbs_navlinks_s
 35. Imran Din M, Mirza ML, Ata S, Athar M, Mohsin IU. Thermodynamics of biosorption for removal of Co(II) ions by an efficient and ecofriendly biosorbent (saccharum bengalense): Kinetics and isotherm modeling. *J Chem*. 2013;2013.
 36. Karthik V, Saravanan K, Sivarajasekar N, Suriyanarayanan N. Bioremediation of dye bearing effluents using microbial biomass. *Ecol Environ Conserv*. 2016;22.
 37. Park D, Yun YS, Park JM. The past, present, and future trends of biosorption. *Biotechnol Bioprocess Eng*. 2010;15(1):86–102.
 38. Won SW, Han MH, Yun Y sang. Different binding mechanisms in biosorption of reactive dyes according to their reactivity. *Water Res*. 2008;42(19):4847–55.
 39. Siddeeg SM, Tahoon MA, Rebah FB. Agro-industrial waste materials and wastewater as growth media for microbial biofloculants production: a review. *Mater Res Express*. 2019 Dec;7(1):012001.
 40. Brierley J, Brierley C, Goyak GM. AMT-Bioclain: a new wastewater treatment and metal recovery technology. *No Source Inf Available*. 1986 Jan 1;4.
 41. Rohatgi A. WebPlotDigitizer User Manual. [Http://rohatgi.info/WebPlotDigitizerapp](http://rohatgi.info/WebPlotDigitizerapp) Accessed June 2 2014. 2013;1–17.
 42. Salvi NA, Chattopadhyay S. Biosorption of Azo dyes by spent *Rhizopus arrhizus* biomass. *Appl Water Sci*. 2017 Oct 1;7(6):3041–54.
 43. Tran H. Differences between Chemical Reaction Kinetics and Adsorption Kinetics: Fundamentals and Discussion. 2022 Jun 22;
 44. Mat Lazim Z, Hadibarata T, Puteh M, Yusop Z, Wirasmita R, Mohd Nor N. Utilization of durian peel as potential adsorbent for bisphenol a removal in aqueous solution. *J Teknol*. 2015 Jul 1;74:109–15.
 45. Alharbi HA, Hameed BH, Alotaibi KD, Aloud SS, Al-Modaihsh AS. Mesoporous Activated Carbon from Leaf Sheath Date Palm Fibers by Microwave-Assisted Phosphoric Acid Activation for Efficient Dye Adsorption. *ACS Omega*. 2022 Dec 20;7(50):46079–89.
 46. Fonseca GC da, Oliveira MS, Martins CVC, de Souza JCP. How the Carbonization Time of Sugarcane Biomass Affects the Microstructure of Biochar and the Adsorption Process? *Sustainability*. 2022 Jan;14(3):1571.
 47. Lagergren, S. About the theory of so-called adsorption of soluble substances. *Kongliga Sven Vetenskapsakademiens Handl*. 1898;24(4):1–39.
 48. Ho YS, McKay G. Sorption of Dye From Aqueous Solution by Peat. *Chem Eng J*. 1998 Jun 1;70:115–24.
 49. Ho YS, McKay G. The kinetics of sorption of basic dyes from aqueous solution by sphagnum moss peat. *Can J Chem Eng*. 1998;76(4):822–7.
 50. Febrianto J, Kosasih AN, Sunarjo J, Ju YH, Indraswati N, Ismadji S. Equilibrium and kinetic studies in adsorption of heavy metals using biosorbent: A summary of recent studies. *J Hazard Mater*. 2009;162(2–3):616–45.
 51. Tran HN, You SJ, Hosseini-Bandegharaei A, Chao HP. Mistakes and inconsistencies regarding adsorption of contaminants from aqueous solutions: A critical review. *Water Res*. 2017 Sep 1;120:88–116.

52. Lagergren S, Svenska K. , "About the theory of so-called adsorption of soluble substances, Zur theorie der sogenannten adsorption gel?ster stoffe,." *Vetenskapsakademiens Handl.* 1898;24:1-39.
53. Blanchard G, Maunaye M, Martin G. *Water Res.* 1984;18:1501-7.
54. Ho YS, McKay G. Pseudo-second order model for sorption processes. *Process Biochem.* 1999 Jul;34(5):451-65.
55. Cope FW. Generalizations of the Roginsky-Zeldovich (or Elovich) equation for charge transport across biological surfaces. *Bull Math Biophys.* 1972 Sep 1;34(3):419-27.
56. Marczewski AW. Application of mixed order rate equations to adsorption of methylene blue on mesoporous carbons. *Appl Surf Sci.* 2010;256(17):5145-52.
57. Hu Q, Pang S, Wang D. In-depth Insights into Mathematical Characteristics, Selection Criteria and Common Mistakes of Adsorption Kinetic Models: A Critical Review. *Sep Purif Rev.* 2021 Jul 1;0(0):1-19.
58. Haerifar M, Azizian S. Fractal-Like Kinetics for Adsorption on Heterogeneous Solid Surfaces. *J Phys Chem C.* 2014 Jan 6;118:1129-34.
59. Tseng RL, Wu PH, Wu FC, Juang RS. A convenient method to determine kinetic parameters of adsorption processes by nonlinear regression of pseudo-nth-order equation. *Chem Eng J.* 2014 Feb 1;237:153-61.
60. Weng CH, Pan YF. Adsorption characteristics of methylene blue from aqueous solution by sludge ash. *Colloids Surf Physicochem Eng Asp.* 2006 Feb 15;274(1):154-62.
61. Kuo S, Lotse E. Kinetics of phosphate adsorption and desorption by hematite and gibbsite I. *Soil Sci.* 1973 Dec 1;116:400-6.
62. Avrami M. Kinetics of Phase Change. II Transformation-Time Relations for Random Distribution of Nuclei. *J Chem Phys.* 1940 Feb 1;8:212-24.
63. Haerifar M, Azizian S. An exponential kinetic model for adsorption at solid/solution interface. *Chem Eng J.* 2013 Jan 15;215-216:65-71.
64. Wilczak A, Keinath T. Kinetics of sorption and desorption of copper(II) and lead(II) on activated carbon. *Water Environ Res.* 1993 May 1;65:238-44.
65. Eris S, Azizian S. Analysis of adsorption kinetics at solid/solution interface using a hyperbolic tangent model. *J Mol Liq.* 2017 Feb 1;231.
66. Brouers F, Al-Musawi TJ. Brouers-Sotolongo fractal kinetics versus fractional derivative kinetics: A new strategy to analyze the pollutants sorption kinetics in porous materials. *J Hazard Mater.* 2018 May 15;350:162-8.
67. Brouers F, Sotolongo-Costa O. Generalized fractal kinetics in complex systems (application to biophysics and biotechnology). *Phys Stat Mech Its Appl.* 2006;368(1):165-75.
68. Nayak AK, Pal A. Development and validation of an adsorption kinetic model at solid-liquid interface using normalized Gudermannian function. *J Mol Liq.* 2019 Feb 15;276:67-77.
69. Lawal WA, Choi H. Feasibility Study on the Removal of Perfluorooctanoic Acid by Using Palladium-Doped Nanoscale Zerovalent Iron. *J Environ Eng.* 2018 Nov 1;144(11):04018115.
70. Wayman M, Tseng MC. Inhibition-threshold substrate concentrations. *Biotechnol Bioeng.* 1976;18(3):383-7.
71. Głuszczyk P, Petera J, Ledakowicz S. Mathematical modeling of the integrated process of mercury bioremediation in the industrial bioreactor. *Bioprocess Biosyst Eng.* 2011;34(3):275-85.
72. Kass RE, Raftery AE. Bayes Factors. *J Am Stat Assoc.* 1995 Jun 1;90(430):773-95.
73. Burnham KP, Anderson DR. *Model Selection and Multimodel Inference: A Practical Information-Theoretic Approach.* Springer Science & Business Media; 2002. 528 p.
74. Foo KY, Hameed BH. Textural porosity, surface chemistry and adsorptive properties of durian shell derived activated carbon prepared by microwave assisted NaOH activation. *Chem Eng J.* 2012 Apr;187:53-62.
75. Kebir M, Trari M, Maachi R, Nasrallah N, Amrane A. Valorization of *Inula viscosa* waste extraction, modeling of isotherm, and kinetic for the tartrazine dye adsorption. *Desalination Water Treat.* 2015 Jun 1;54.
76. Chukwuemeka-Okorie HO, Ekuma FK, Akpomie KG, Nnaji JC, Okerefor AG. Adsorption of tartrazine and sunset yellow anionic dyes onto activated carbon derived from cassava sievate biomass. *Appl Water Sci.* 2021;11(2).
77. Gautam PK, Shivapriya PM, Banerjee S, Sahoo AK, Samanta SK. Biogenic fabrication of iron nanoadsorbents from mixed waste biomass for aqueous phase removal of alizarin red S and tartrazine: Kinetics, isotherm, and thermodynamic investigation. *Environ Prog Sustain Energy.* 2020;39(2).
78. Goscianska J, Ciesielczyk F. Lanthanum enriched aminosilane-grafted mesoporous carbon material for efficient adsorption of tartrazine azo dye. *Microporous Mesoporous Mater.* 2019;280:7-19.
79. Mirzajani R, Karimi S. Ultrasonic assisted synthesis of magnetic Ni-Ag bimetallic nanoparticles supported on reduced graphene oxide for sonochemical simultaneous removal of sunset yellow and tartrazine dyes by response surface optimization: Application of derivative spectrophotometry. *Ultrason Sonochem.* 2019;50:239-50.
80. Torres-Pérez J, Muñoz-Armenta G, Réyes-López SY. Effect of microwave treatment onto activated carbon produced from pecan nut shells for Tartrazine removal from aqueous media. *Int J Environ Pollut.* 2018;63(4):298-319.
81. Albadarin AB, Charara M, Abu Tarboush BJ, Ahmad MNM, Kurniawan TA, Naushad M, et al. Mechanism analysis of tartrazine biosorption onto masau stones; a low cost by-product from semi-arid regions. *J Mol Liq.* 2017;242:478-83.
82. Gautam RK, Banerjee S, Sanroman MA, Chattopadhyaya MC. Synthesis of copper coordinated dithiooxamide metal organic framework and its performance assessment in the adsorptive removal of tartrazine from water. *J Environ Chem Eng.* 2017;5(1):328-40.
83. Bacioiu IG, Stoica L, Constantin C, Stanescu AM. Adsorption equilibrium and kinetics modeling for tartrazine(E102) - Fe(II) based adsorbent system. *Rev Chim.* 2016;67(12):2391-5.
84. Alcántara-Cobos A, Solache-Ríos MJ, Díaz-Nava MDC. Adsorption of tartrazine on an iron modified zeolitic tuff. *Environ Eng Manag J.* 2016;15(11):2453-8.
85. Gautam PK, Gautam RK, Banerjee S, Lofrano G, Sanroman MA, Chattopadhyaya MC, et al. Preparation of activated carbon from Alligator weed (*Alternanthera philoxeroides*) and its application for tartrazine removal: Isotherm, kinetics and spectroscopic analysis. *J Environ Chem Eng.* 2015;3(4):2560-8.
86. Ansari R, Keivani MB, Delavar AF. Application of polyaniline nanolayer composite for removal of tartrazine dye from aqueous solutions. *J Polym Res.* 2011;18(6):1931-9.
87. Rodríguez-Zapién KV, Torres-Pérez J, Reyes-López SY. Environmental application of quartz-based construction waste: tartrazine removal from aqueous media. *Int J Environ Sci Technol.* 2022;19(10):10381-92.
88. Balayeva OO, Azizov AA, Muradov MB, Alosmanov RM. Removal of tartrazine, ponceau 4R and patent blue V hazardous food dyes from aqueous solutions with ZnAl-LDH/PVA nanocomposite. *J Dispers Sci Technol.* 2021;
89. Foo KY, Hameed BH. Insights into the modeling of adsorption isotherm systems. *Chem Eng J.* 2010;156(1):2-10.
90. Yaneva ZL, Georgieva NV. Insights into Congo Red adsorption on agro-industrial materials - spectral. *Int Rev Chem Eng.* 2012;4(2):127-46.
91. Azizian S. Kinetic models of sorption: A theoretical analysis. *J Colloid Interface Sci.* 2004;276(1):47-52.
92. Tykodi R. Kinetics and thermodynamics of adsorption of dyes on activated carbon fibers. *J Environ Manage.* 2004;71(4):305-15.
93. Lin J, Wang Y. Kinetics of adsorption of dyes from aqueous solution onto modified corn straw. *J Hazard Mater.* 2009;161(2-3):923-8.
94. Simonin O. Kinetics and thermodynamics of adsorption of dyes on activated carbon fibers. *J Environ Manage.* 2016;181:100-9.
95. Hu Y, Li L, Wang Y. Kinetics of adsorption of anionic and cationic dyes on biochar. *J Environ Manage.* 2018;212:166-74.
96. Moussout N, Simonin O, Leclère Q. Kinetics and thermodynamics of adsorption of anionic and cationic dyes on biochars. *J Environ Manage.* 2018;210:112-20.
97. Ho YS, McKay G, Healy TW. The intraparticle diffusion model applied to adsorption systems. *J Colloid Interface Sci.* 2000;230(2):117-25.
98. Plazinski J, Rudzinski W. Kinetics of adsorption of dyes from aqueous solutions on activated carbon. *J Colloid Interface Sci.* 2009;335(2):476-81.

99. Gautam RK, Gautam PK, Banerjee S, Rawat V, Soni S, Sharma SK, et al. Removal of tartrazine by activated carbon biosorbents of *Lantana camara*: Kinetics, equilibrium modeling and spectroscopic analysis. *J Environ Chem Eng*. 2015;3(1):79–88.
100. Wan Ngah WS, Ariff NFM, Hanafiah MAKM. Preparation, Characterization, and Environmental Application of Crosslinked Chitosan-Coated Bentonite for Tartrazine Adsorption from Aqueous Solutions. *Water Air Soil Pollut*. 2010 Feb 1;206(1):225–36.
101. Mittal A, Kurup L, Mittal J. Freundlich and Langmuir adsorption isotherms and kinetics for the removal of Tartrazine from aqueous solutions using hen feathers. *J Hazard Mater*. 2007;146(1–2):243–8.
102. Mittal A, Mittal J, Kurup L. Adsorption isotherms, kinetics and column operations for the removal of hazardous dye, Tartrazine from aqueous solutions using waste materials—Bottom Ash and De-Oiled Soya, as adsorbents. *J Hazard Mater*. 2006 Aug 25;136(3):567–78.
103. Dotto GL, Vieira MLG, Pinto LAA. Kinetics and Mechanism of Tartrazine Adsorption onto Chitin and Chitosan. *Ind Eng Chem Res*. 2012 May 16;51(19):6862–8.